


Article

Photochromism, UV-Vis, Vibrational and Fluorescence Spectroscopy of Differently Colored Hackmanite

Chuchu Song¹, Qingfeng Guo^{1,*} , Yang Liu¹, Yinghua Rao¹ and Libing Liao^{2,*}

¹ School of Gemology, China University of Geosciences, Beijing 100083, China; 1009221214@email.cugb.edu.cn (C.S.); 200922004@email.cugb.edu.cn (Y.L.); 2109220008@email.cugb.edu.cn (Y.R.)

² Beijing Key Laboratory of Materials Utilization of Nonmetallic Minerals and Solid Wastes, National Laboratory of Mineral Materials, School of Materials Sciences and Technology, China University of Geosciences, Beijing 100083, China

* Correspondence: qfguo@cugb.edu.cn (Q.G.); clayl@cugb.edu.cn (L.L.)

Abstract: Because of the rich fluorescent color and unique photochromic properties, hackmanite has attracted many mineralogists. In this paper, the basic gemmological characteristics and photochromic and fluorescence mechanisms of four different colors of hackmanite are further investigated through the study of their structural, compositional, and spectroscopic features. The results show the change in the color of hackmanite in photochromism is caused by the joint action of the F-center and the oxygen hole centers. The change in the UV-Vis spectra may be caused by the superposition of two peaks. Under 365 nm UV excitation, the peak of fluorescence spectra of 662 nm is related to the ${}^2\Pi_g \rightarrow {}^2\Pi_u$ transition of S_2^- , the blue emission at 441 nm is caused by the ${}^3P_{0,1} \rightarrow {}^1S_0$ transition of s^2 ions (Pb^{2+} , Tl^+ , Sn^{2+} , Sb^{2+}), and at 541 nm is caused by the Mn^{2+} center. The results are helpful in deepening the understanding of photochromism, fluorescence mechanism, and its structure, expanding the application of hackmanite.

Keywords: hackmanite; mineralogy; photochromism; infrared spectra; fluorescence mechanism



Citation: Song, C.; Guo, Q.; Liu, Y.; Rao, Y.; Liao, L. Photochromism, UV-Vis, Vibrational and Fluorescence Spectroscopy of Differently Colored Hackmanite. *Crystals* **2023**, *13*, 1607. <https://doi.org/10.3390/cryst13111607>

Academic Editor: Sergey V. Krivovichev

Received: 17 October 2023

Revised: 14 November 2023

Accepted: 17 November 2023

Published: 20 November 2023



Copyright: © 2023 by the authors. Licensee MDPI, Basel, Switzerland. This article is an open access article distributed under the terms and conditions of the Creative Commons Attribution (CC BY) license (<https://creativecommons.org/licenses/by/4.0/>).

1. Introduction

Hackmanite is a feldspar-like mineral, and gem-grade hackmanite is well known for its charming photochromism. The structure of the hackmanite ($Na_8Al_6Si_6O_{24}(Cl, S)_2$) consists of a tetrahedron of AlO_4 and SiO_4 alternating with four and six members. The framework has a large cavity containing Cl^- and Na^+ ion forming $(Na_4Cl)^{3+}$ entities, where Na coordinates with three O^{2-} ions and one Cl^- in the frame (Figure 1) [1,2]. Infrared spectroscopy studies show that the spectra below 150 cm^{-1} belong to Na_4Cl tetrahedron, the peaks between 150 and 300 cm^{-1} are related to the Al-Si skeleton, and the peaks around 735 cm^{-1} are related to the symmetric stretching vibration of T-O-T (T = Al and Si) [3–5]. The synthesized $Na_8Al_6Si_6O_{24}(Cl, S)_2$ sample showed a typical peak (about 450 cm^{-1}) and symmetric (about 700 cm^{-1}) and asymmetric (about 1000 cm^{-1}) T-O-T peaks (T = Al and Si). Under irradiation at 365 nm, the FTIR (Fourier transform infrared) spectra basically do not change, while under irradiation at 254 nm, the FTIR spectra change a little, but it can be observed, especially in the asymmetry T-O-T signal [6]. However, there are still no specific reports on the relationship between the structure of natural hackmanite and its photochromic properties.

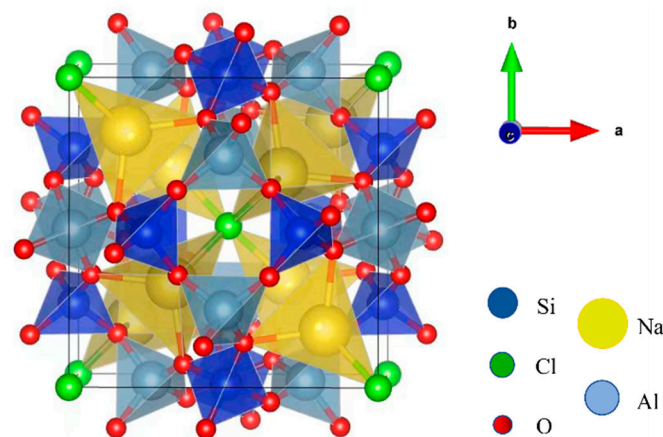


Figure 1. The structure of hackmanite unit cell [7] (a is the y-axis, b is the x-axis, and c is the z-axis).

Photochromism occurs in hackmanite after short-wave or long-wave ultraviolet irradiation. The present study shows that it is due to the fact that S substitutes for Cl in the sodalite and forms Cl vacancy. However, the sulfur-containing ion is unstable when it has Cl vacancy around it, and it is easy to decompose when irradiated by ultraviolet light. The electrons generated in this process are excited under the UV light about 4.3~5.5 eV, entering the conduction band and captured by Cl vacancy, which is relatively stable to form an F-center, resulting in a purple color [8–13]. The band gap is about 7.7 eV, and the main types of sulfur ions in hackmanite are S_2^{2-} or S^{2-} , which provide electrons for photochromism [8]. However, the specific sulfur-containing ion that causes its photochromism has not been determined yet [6]. The effect of other elements, except S, on photochromism is still controversial [8–13].

Both violet square sodalite showed orange-red fluorescence and orange-violet-red fluorescence by UV irradiation. In hackmanite, green fluorescence is thought to be caused by partial substitution of Na^+ by Mn, while partial substitution of Al^{3+} by Fe^{3+} leads to red luminescence and orange fluorescence is caused by the S_2^- [13–15]. Ce^{3+} causes the fluorescence spectra to show an emission peak around 340 nm, Eu^{2+} leads to violet fluorescence, and the s^2 -type ions are associated with blue fluorescence, while the association of Ti^{3+} with oxygen vacancies may also lead to blue fluorescence [16].

In addition to its beautiful appearance, attractive fluorescent color, and photochromic characteristics, natural hackmanite is also of industrial importance [5,10]. Until now, most of the studies have been on synthetic hackmanite, and the fluorescence and photochromic properties of natural hackmanite, as well as the relationship between photochromic and fine structure, have not been systematically studied. Natural hackmanite differs from synthetic hackmanite in many ways in its EPR profile, especially in the location of oxygen holes. The signal of oxygen vacancies is generally not observed in synthetic samples. Therefore, in this paper, 14 natural hackmanite samples were selected to comprehensively discuss the composition, structure, photochromism, and fluorescent properties. The natural hackmanite has the effect of other elements on photochromism, which was also observed in the experiment. Plus, the synthesis of hackmanite is mainly focused on the F-center, and the article is aimed at exploring the effect of oxygen holes on the photochromic properties to provide new ideas for the synthesis of hackmanite energy storage materials. This study is also helpful in systematically understanding the gemological characteristics, optical properties, and internal structure of natural hackmanite, broadening its application in various fields of optical data storage, security marking, medical diagnostics, and so on [6,17].

2. Materials and Methods

2.1. Materials

14 hackmanite samples from Afghanistan, numbered s-1~s-14, were selected for the experiment, as shown in Figure 2a. s-1, s-9, and s-13 are light purple, s-2, 7 are pink purple, s-3, 10, and 11 are blue, s-4, s-6 are dark purple, s-5 is white, and s-8, s-12, and s-14 are mostly purple and contain white minerals. The samples are all mineral combination, which is granular structure and blocky constructure.

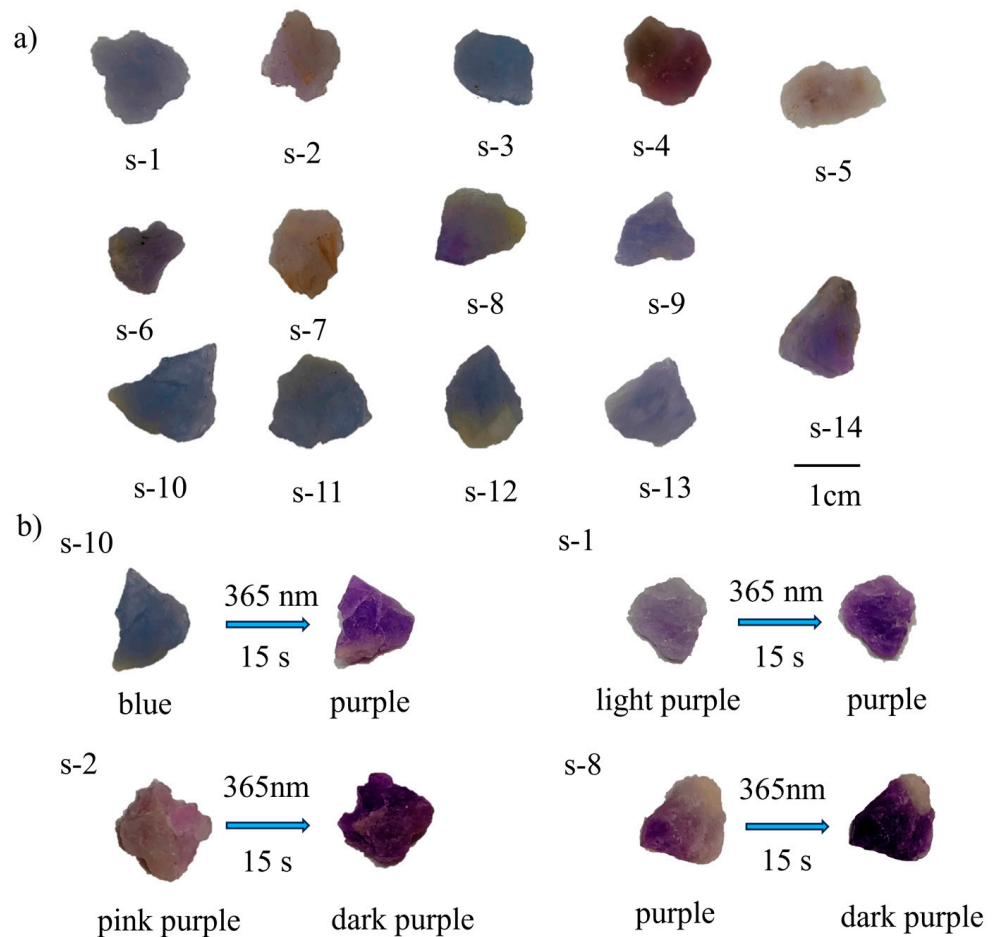


Figure 2. (a) Appearance of hackmanite samples, (b) Color change of hackmanite samples after exposure to 365 nm UV fluorescent lamp for 15 s.

The photochromic color change was present in all the samples of hackmanite. Under the irradiation of a 365 nm UV fluorescent lamp (60 W), the samples changed color rapidly, and the time of color change was very short, less than 1 s. Figure 2b shows the photochromic color change of the samples, and the selected samples are the representative samples of different color shades. The color changes of differently colored hackmanites are different: blue hackmanite changes to purple, light purple hackmanite changes to purple, pink-purple hackmanite changes to dark purple, and purple hackmanite changes to dark purple.

2.2. Methods

Routine gemological characterization tests were performed using a gemological microscope, electronic balance, refractometer, and UV fluorescent lamp. Infrared spectroscopic testing was performed using a Tensor 27 Fourier infrared spectrometer using the reflectance method. The test voltage is 220 V, the resolution is 4 cm^{-1} , the scanning range is $1800\text{--}400\text{ cm}^{-1}$, and the scanning speed is 10 kHz. The UV-Vis spectral test is performed using UV-3600 UV-Visible spectrophotometer of Shimadzu, Japan. The test method was re-

flectance, the test range was 200–900 nm, and the sampling interval was 0.5 s. Fluorescence spectra were tested using a Hitachi F-4700 instrument to test the fluorescence emission spectra of the samples. The test was carried out using a PMT voltage of 600 V, a scanning speed of 12,000 nm/min, and the test range was 390–680 nm. The EPR results were obtained with a paramagnetic resonance spectrometer ESR/EPR (A300, Bruker, Germany) under the following test conditions: room temperature, 20.03 mW power, and 100 kHz modulation frequency. The trace element test was carried out by laser ablation inductively coupled plasma mass spectrometry (LA-ICP-MS) using Analytik Jena Plasma Quant MS, (Jena, Germany). The laser ablation system was an excimer laser with a resolution of 193 nm. High-purity helium was used as a carrier gas for the experiments. The single-point analysis time was 85 s, of which the blank background acquisition time was 20 s, the continuous ablation acquisition time was 45 s, and the time for cleaning the sampling system was 40 s. The data point size of the sample acquisition was 100 μm . The electron probe test was performed using an EPMA-1600 electron probe microanalyzer manufactured by Shimadzu Corporation of Ishi, Shimadzu, Japan. The accelerating voltage was 15 kV, the current was 10 nA, the electron beam spot diameter was 5 μm , the sample surface was sprayed with carbon, SPI standard samples, and the ZAF calibration method was used for data processing.

3. Results and Discussion

3.1. Basic Gemological Characteristics

Photochromism was found in all hackmanite samples. Under the irradiation of a 365 nm UV fluorescent lamp (60 W), the color of hackmanite samples changed rapidly, and the time was less than 1 s (Figure 2b). Figure 2b shows the photochromism of hackmanite samples, which varies with different colors.

There are a large number of uneven fractures on the surface of hackmanite samples (Figure 3a,c), and a group of moderate cleavage is developed. The symbiotic minerals of hackmanite were observed to be white, and some developed in bands (Figure 3b,d). The refractive index of the sample ranges from 1.482 to 1.485, and the relative density ranges from 2.26 to 2.36 (Table S1). All hackmanite samples have fluorescence under long-wave ultraviolet lamps (Figure S1) but do not have fluorescence under short-wave ultraviolet lamps. All hackmanite samples were phosphorescent-free. The gas-liquid fluid inclusions developed in the hackmanite samples (Figure 3f), and there was a group of medium cleavage (Figure 3e), which was fully bright under orthogonal polarization, indicating that it was a mineral aggregate.

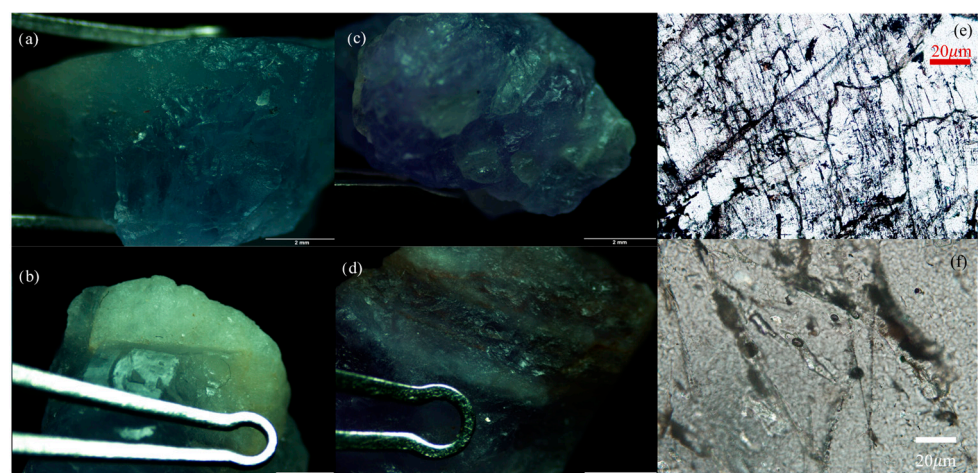


Figure 3. Characteristics of hackmanite under gemological microscope. (a,c) Uneven ports developed by hackmanite, (b,d) Other minerals associated with hackmanite. Characteristics of hackmanite samples under a polarizing microscope, (e) A set of medium cleavage of hackmanite, (f) Fluid inclusions.

3.2. Structure and Composition Characteristics

The crystal structure of the tetrahedral framework SOD ($[\text{Al}_6\text{Si}_6\text{O}_{24}]^{6-}$) with large cavities (β cages) within the structure can accommodate large cations such as Na^+ , K^+ , and Ca^{2+} and additional anions such as Cl^- , F^- , SO_4^{2-} , S^{2-} , S^{3-} , CO_3^{2-} , OH^- [18]. As shown in Figure 4, the absorption peak at 1008 cm^{-1} is due to the asymmetric stretching vibration of Si-O-Si, and its wave number changes due to the difference of Si/Al in the framework [19–21]; 734, 709, and 665 cm^{-1} correspond to the vibrational peaks of the symmetric Si-O-Si, and another study suggests that 709 cm^{-1} corresponds to the bending vibration of the chemical bonding in the O-Al-O unit due to the Al-induced chemical bond bending vibrations; 665 cm^{-1} is caused by Al-O vibrations, and the peaks at 474 and 439 cm^{-1} belong to the bending vibrations of T-O-T (T = Si/Al) [8,22–30].

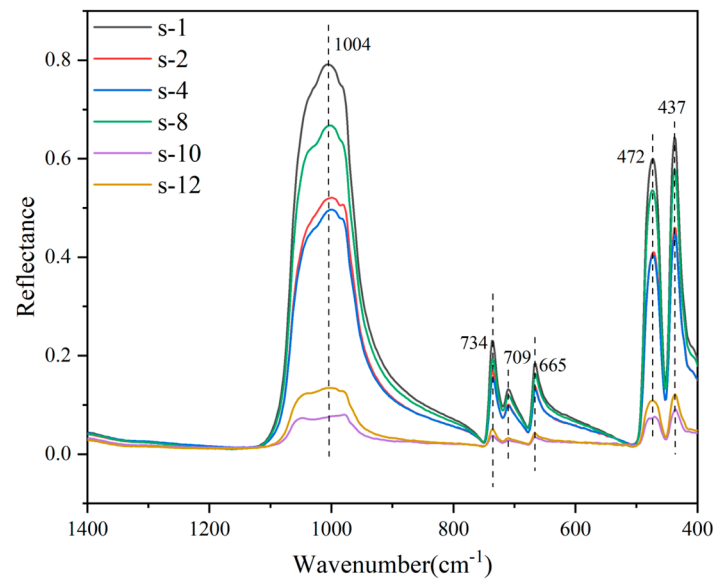


Figure 4. FTIR spectra of hackmanite samples.

In order to explore the microscopic phase composition of different colors of hackmanite, Raman spectra of blue and purple hackmanite were tested, and the results are shown in Figure 5. It is observed that s-10 and s-12 have peaks at 167, 265, 294, 463, 987, and 1062 cm^{-1} , which are consistent with RRUFF ID R040141.

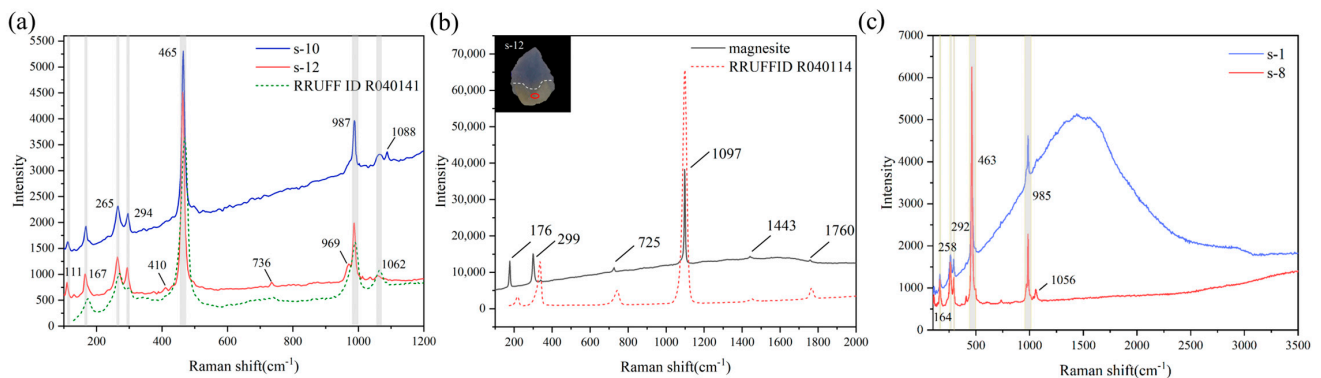


Figure 5. Raman spectra of hackmanite samples. (a) The main gemstone of hackmanite, (b) The Raman spectra of magnesite and the red areas are tested points. (c) The Raman spectra of the main gemstone of hackmanite of $200\text{--}3500\text{ cm}^{-1}$.

The results show that the peak at 167 cm^{-1} is caused by cationic sublattice vibration, and 265 cm^{-1} is caused by Na-O with Al/Si-tetrahedra bending or ν_2 vibration of S^{3-} . The

peak at 294 cm^{-1} is caused by the symmetric Al/Si-tetrahedra bending, and the peak at 463 cm^{-1} is caused by the Na_4Cl -tetrahedra stretching, Si-O bending, SiO_4 vibration or ν of T-O-T; 987 cm^{-1} represents the A_1 stretching frequency of ν_1 of sodalite framework or the symmetric Al/Si-tetrahedra stretching. The literature suggests that the peak at 987 cm^{-1} may also be caused by the oxygen bending mode A_1 or the symmetric stretching vibration of $A_1(\nu_1)\text{SO}_4^{2-}$; 1062 cm^{-1} is caused by asymmetric Al/Si-tetrahedra stretching and is also the main energy band of CO_3^{2-} [17,25,30–32].

Unlike other samples, the s-12 also has peaks at 410 , 736 , and 969 cm^{-1} . The peak at 410 cm^{-1} is caused by the anti-phase mode E of ν_2 frequency of the framework tetrahedra. The peak at 736 cm^{-1} represents the ν_4 bending frequency of the T_2 mode of the framework; 969 cm^{-1} is caused by the asymmetric strong Si and weak Al-tetrahedra stretching. The s-10 has a peak at 1088 cm^{-1} , which is caused by the $2' \nu_1$ of S^{3-} [17]. The white part of s-12 was significantly different from the main part on magnification examination, and Raman spectra showed that it was not hackmanite but magnesite.

In order to explore the HS^- , the Raman spectra of the main gemstone of hackmanite of $1200\sim 3500\text{ cm}^{-1}$ were tested. However, we did not find obvious signals around the range (Figure 5c).

In order to explore the differences in the composition of different colors of hackmanite, X-ray fluorescence spectroscopy and electron probe tests were carried out, and the results are shown in Table S2 and Table 1. LA-ICP-MS test was used to investigate the trace element composition of hackmanite (the results are shown in Figure 6 and Table S3).

Table 1. EPMA data of hackmanite samples (wt %).

Data	Na_2O	Cr_2O_3	SiO_2	TiO_2	MgO	Fe_2O_3	S	MnO	Al_2O_3	Cl	NiO	K_2O	CaO	Total ¹
s-13-1	24.86	0.00	36.47	0.00	0.01	0	0.1	0.00	31.69	7.21	0.00	0.48	0.09	99.28
s-13-3	24.91	0.00	36.99	0.00	0.00	0.02	0.07	0.01	30.59	7.07	0.02	0.45	0.08	98.61
s-5-1	23.21	0.00	36.96	0.00	0.00	0.08	0.1	0.00	32.78	7.32	0.00	0.23	0.05	99.08
s-5-3	24.93	0.00	37.17	0.00	0.02	0.09	0.08	0.01	31.47	7.01	0.05	0.31	0.09	99.65
s-11-1	23.76	0.02	36.39	0.06	0.00	0.06	0.12	0.05	32.10	7.20	0.00	0.23	0.11	98.47
s-11-2	25.19	0.00	37.25	0.00	0.00	0	0.11	0.03	29.85	6.91	0.08	0.21	0.08	98.15
s-11-3	24.56	0.01	36.60	0.00	0.00	0	0.13	0.00	32.74	7.51	0.02	0.17	0.06	100.10
s-14-2	23.70	0.00	36.58	0.12	0.00	0.07	0.09	0.00	32.67	6.99	0.00	0.29	0.10	99.03
s-14-3	24.88	0.00	37.22	0.01	0.00	0.01	0.10	0.02	31.44	6.99	0.00	0.38	0.08	99.55

¹ In the total sums, oxygen equivalents of Cl are subtracted.

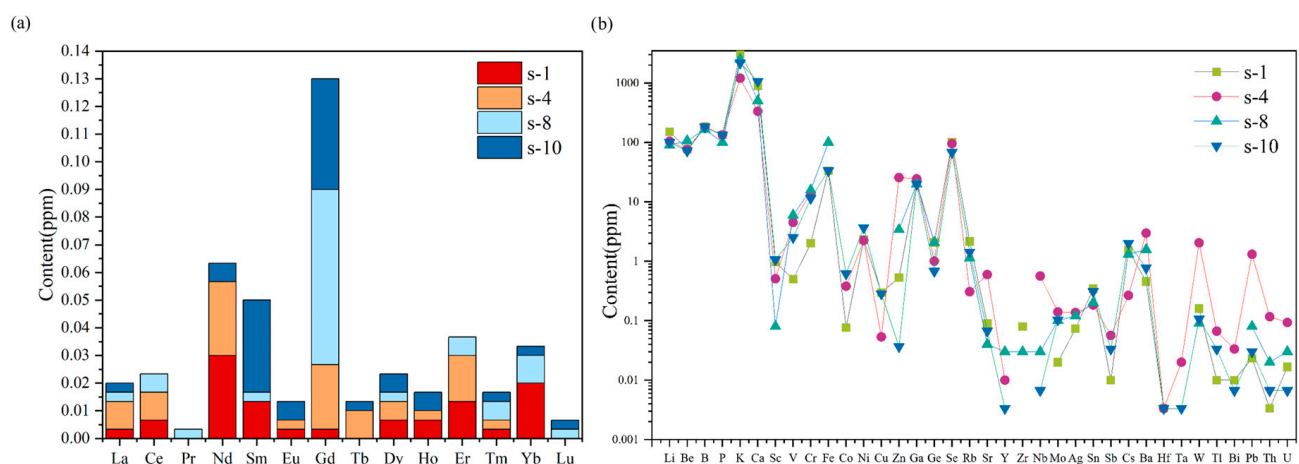


Figure 6. Statistical diagram of trace elements content in hackmanite samples, (a) Statistical diagram of rare earth elements content in hackmanite samples, (b) Statistical diagram of other trace elements content in hackmanite samples.

The content of major elements of hackmanite samples are Na, Al, Si, S, Cl, and O. In addition, there are metallic elements (Ca, K, Mg, Ta, Sr, Ir, Hg), transition metal elements (Fe, Ni, Cu, Mn, Rb, Ba, Hf, Os, Pt, Cr, Sc, Ti), non-metallic elements (Br, As), rare earth elements (Eu, Gd, Tb, Dy, Ho, Er, Tm, Yb, etc.). The average content of Na₂O of light purple, white, blue, and purple sodalite is 24.74%, 24.417%, 24.50%, and 20.26%, and the average Al₂O₃ content is 31.89%, 31.39%, 31.56%, and 21.84%. The average content of SiO₂ is 36.64%, 36.98%, 36.74%, and 48.38%, the average content of SO₃ is 0.20%, 0.21%, 0.30%, and 0.25%, and the average content of Cl is 7.10%, 7.10%, 7.10%, and 4.67%. Purple hackmanite has the lowest Cl content, the lowest Al content, the lowest Na content, and the highest Si content. Blue hackmanite has the highest sulfur content. The colors of the hackmanite samples range from light to dark, with white, light purple, blue, and purple being the successive hues. Among them, the blue hackmanite has the highest content of S, and the purple hackmanite has the lowest content of Cl, which indicates that the substitution of Cl by S has a great influence on the color of hackmanite. According to Figure 6, the contents of rare earth elements and trace elements in the sample are not necessarily related to the color depth but may be related to the hue of the color of the sample.

3.3. Spectroscopic Characterization Tests

3.3.1. Fluorescence Spectra

In Figure 7a, the peaks at 214 nm and 384 nm are observed, and the $\lambda_{em} = 441$ nm. It shows that the optimal excitation wavelength is under 214 nm.

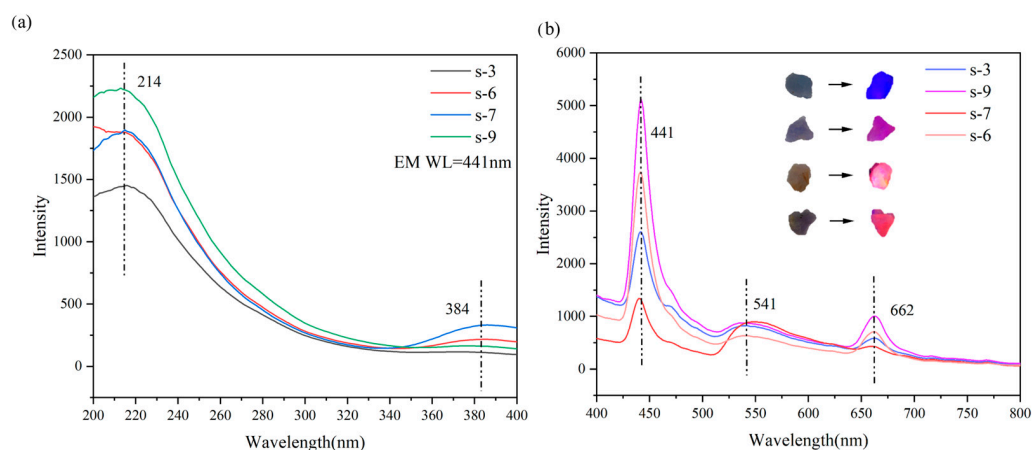


Figure 7. Fluorescence spectra of hackmanite samples, (a) Excitation spectra of hackmanite samples, (b) Emission spectra of hackmanite samples.

All samples fluoresce under a 365 nm long-wave ultraviolet (UV) lamp and vary in colors (Figure S1). And in order to explore the fluorescence emission characteristics of hackmanite, the fluorescence emission spectra under a 384 nm UV lamp were tested (EX slit = 5.0 nm, EM slit = 5.0 nm), using a 500 nm green light filter, as shown in Figure 7b. The fluorescence emission peaks were found at 441, 541, and 662 nm. The emission peak of 662 nm is related to the transition of ${}^2\Pi_g \rightarrow {}^2\Pi_u$ of S_2^- . Some synthetic hackmanite samples also show blue emission at around 441 nm, which is caused by ${}^3P_{0,1} \rightarrow {}^1S_0$ transitions of s^2 -type ions such as Pb^{2+} , Tl^+ , Sn^{2+} , and Sb^{2+} . In other studies, blue fluorescence may be attributed to O^{2-} [2,17,33]. In Table S3, it can be observed that Pb, Tl, Sn, and Sb are present in the hackmanite samples, and it can be inferred that the blue fluorescence is caused by the ${}^3P_{0,1} \rightarrow {}^1S_0$ transition of s^2 ions such as Pb^{2+} , Tl^+ , Sn^{2+} , and Sb^{2+} . The emission front at 541 nm is caused by the Mn^{2+} center, and the presence of Mn can be observed in Table 1. The emission peak of s-9 is most obvious at 441 nm.

3.3.2. UV-Vis Spectra

To examine the photochromism of hackmanite samples, the UV-Vis absorption spectra of the samples were measured. Figure 8a shows that there are absorption peaks in light purple, pink purple, blue, and dark purple samples at around 237, 290, and 540 nm, and from dark purple to blue. The peak at 540 nm shows a red shift, and the peak at 290 nm shows a blue shift. Studies have shown that the substitution of Na^+ by Yb^{3+} and Er^{3+} in synthetic hackmanite will lead to a slight tendency to bluish-purple color [34]. The results of UV-Vis light absorption spectra show that the absorption wavelength of s-10 is larger than that of s-1, s-4, and s-8 around the absorption band of 530~540 nm. According to Figure 6a,b and Table S3, it can be observed that the content of Yb and Er in s-10 is significantly less than that in other samples, which confirms this result.

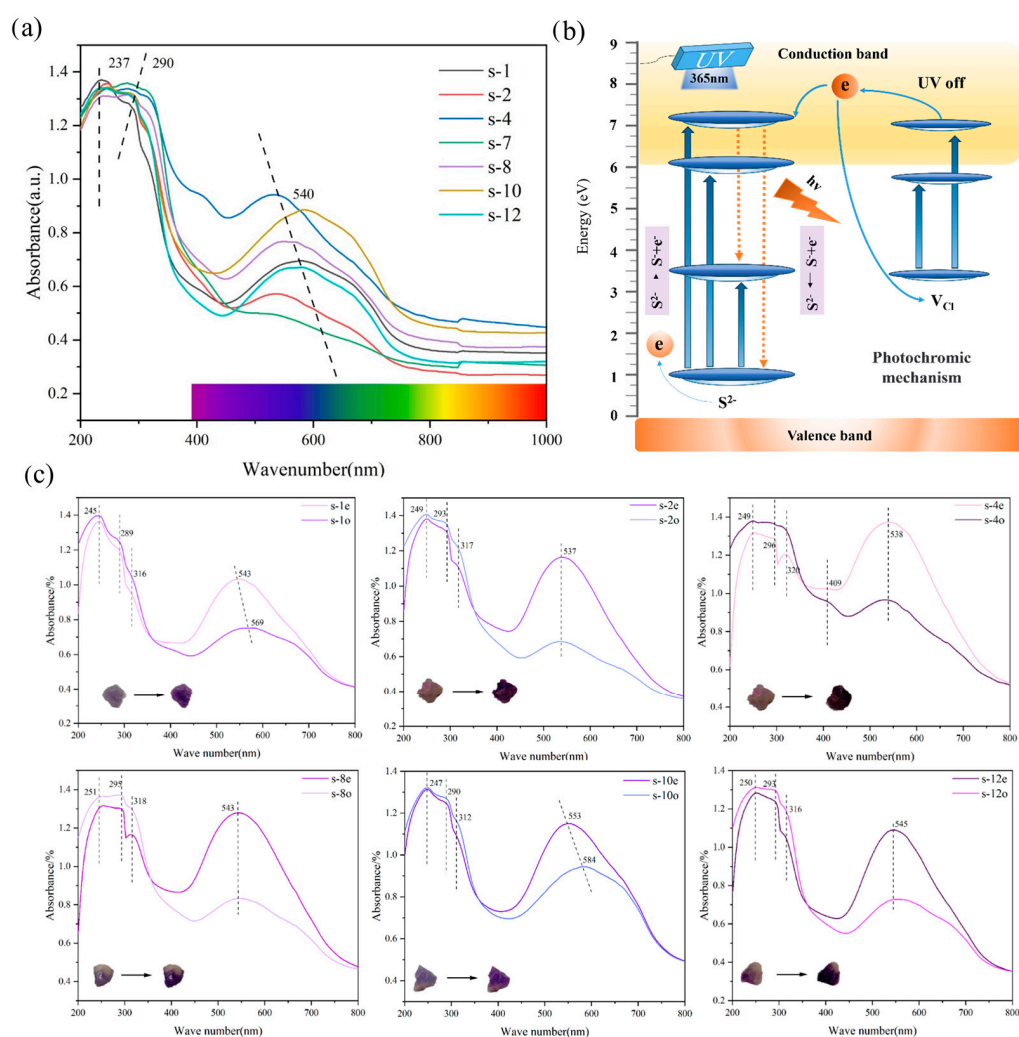


Figure 8. (a) UV-Vis absorption spectra of hackmanite samples, (b) Schematic diagram of hackmanite photochromism mechanism, (c) UV-Vis absorption spectra of hackmanite samples before and after exposure to 365 nm ultraviolet light.

Hackmanite also has a narrow absorption band at 248~295 nm and 310~320 nm caused by $\text{S}^{2-} \rightarrow \text{S}^- + e^- / \text{S}_2^{2-} \rightarrow \text{S}^- + e^-$, which represent the absorption of ultraviolet rays in natural light by S-containing ions. After UVA/UVC irradiation, narrow-band absorption decreased with the increase in irradiation time (Figure 8c and Figure S2). According to Table S2, it can be inferred that most S-containing ions decompose and produce electrons, resulting in weakened ultraviolet absorption after UV irradiation. However, the S content of S-10 is relatively higher, so its absorption intensity weakened relatively smaller.

As shown in Figure 8c, after irradiation of 365 nm and 254 nm ultraviolet lamps, the absorption peak at 540 nm of s-1 and s-10 shifts to a lower number. We selected the absorption-enhanced part of the UV-Vis spectra of s-1 for the split-peak fitting process (Figure 9a,b). It can be observed that there is also a peak near 1.86 eV (667 nm). The peak is less enhanced after photochromism than the peak at 2.23 eV (557 nm). The peak at 2.23 eV (557 nm) and the peak at 1.86 eV (667 nm) before photochromism is caused by the oxygen hole centers [12]. The peak at 1.86 eV (667 nm) after photochromism is caused by F-center [34]. Therefore, the shift of the absorption peaks of s-1 and s-10 after irradiation may be due to the superposition of the two sites.

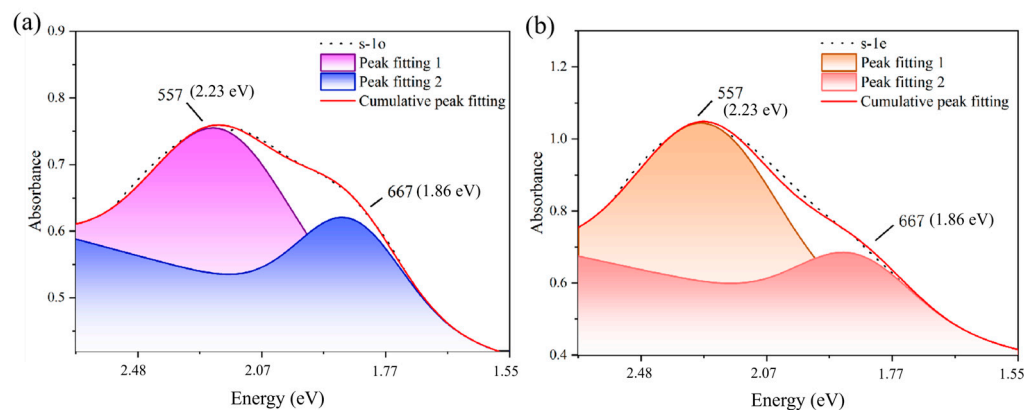


Figure 9. (a) Peak fitting of UV-Vis absorption spectra of s-1 before photochromism, (b) Peak fitting of UV-Vis absorption spectra of s-1 after photochromism.

Usually, the absorption band of 530–540 nm is associated with F-center [8–13]. In natural hackmanite samples, it is generally believed that the photochromism of hackmanite is due to the electrons from sulfide ions trapped in the Cl vacancy, forming F-centers (Figure 8b) [6,13]. As shown in Figure 2b, hackmanite samples showed obvious photochromic phenomena after exposure to 365 nm ultraviolet (UV) lamps. In order to study the photochromic phenomenon, UV-Vis spectra tests were conducted on samples of different colors before and after photochromism (Figure 8c). In Figures 8c and S2, the UV-Vis spectra of all samples showed obvious changes after photochromism under the irradiation of UV lamps at 365 nm and 254 nm. The specific performance is that the absorption band at 540 nm becomes stronger, and the longer the irradiation time under the ultraviolet lamp at 254 nm, the greater the intensity of the absorption band.

In order to further investigate the mechanism of photochromism, the EPR experiment was tested. In Figure 10a,b, it is observed that there is a signal presence of $g = 2.011$, which indicates the presence of oxygen hole centers in hackmanite [35]. The EPR spectra of hackmanite has a strong signal at $g = 2.011$, which also disappears along with the color of the sample when heated to 400 °C [36]. In the experimental results, the signal at $g = 2.011$ corresponds to the light purple color of the samples in natural light; 254 nm UV irradiation leads to photochromism of hackmanite with deepening of the purple color, and correspondingly, the signal at $g = 2.011$ is also significantly enhanced. Based on the result, we can speculate that the photochromic change of hackmanite is not only related to the F-center, but also the oxygen hole centers play a role in the deepening of the purple color of hackmanite. So, the change in the color of hackmanite may be the result of the joint action of the F-center and the oxygen hole centers.

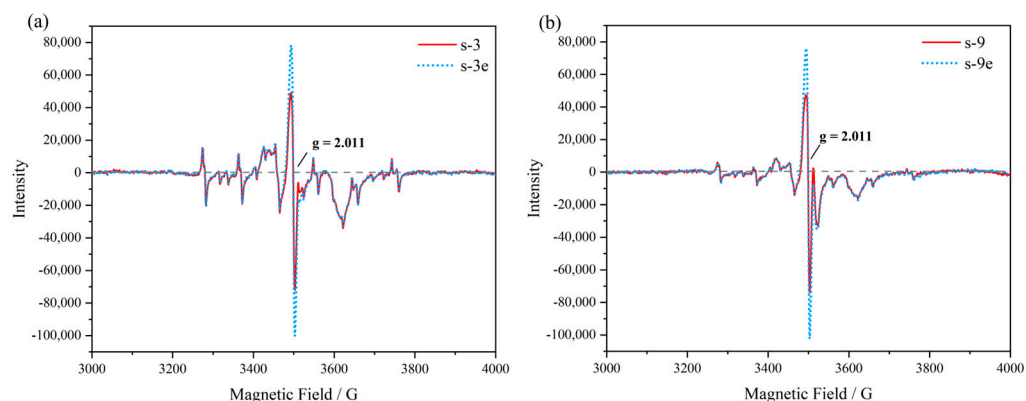


Figure 10. EPR spectra of hackmanite samples. (a) EPR spectra of s-3; (b) EPR spectra of s-9.

4. Conclusions

The major elements of the hackmanite samples of different colors are Na, Al, Si, S, Cl, and O. In addition, there are metallic elements, transition metal elements, non-metallic elements, and rare earth elements. The larger absorption wavelength of s-10 shows that Yb and Er also have an effect on color. The different fluorescence color of hackmanite is caused by different ions, which we have detected the relative elements. The study systematically investigates the basic gemmological properties of the natural hackmanite, complements the study of Raman spectroscopy and fluorescence properties, excludes the possibility of HS^- providing electrons during photochromism of the sample, and investigates the cause of the blue fluorescence emission peaks. Moreover, the first EPR test of natural hackmanite before and after photochromism was performed, and it was hypothesized that the photochromism is the result of the joint action of the F-center and oxygen hole centers, which is helpful to provide ideas for the research of hackmanite as an energy storage materials, deepen the systematic understanding of the hackmanite and broaden the application of hackmanite as photochromic material in various fields.

Supplementary Materials: The following supporting information can be downloaded at: <https://www.mdpi.com/article/10.3390/cryst13111607/s1>, Figure S1: Irradiation of hackmanite samples under 365 nm UV fluorescent lamp; Figure S2: UV-Vis absorption spectra of hackmanite samples before and after exposure to 254 nm ultraviolet light; Table S1: Basic gemmological property parameters of hackmanite samples; Table S2: X-ray Fluorescence spectral analysis data of hackmanite samples (wt %); Table S3: LA-ICP-MS data of hackmanite.

Author Contributions: Performing experiments and writing the original manuscript, C.S.; reviewing and editing, Q.G.; making analysis, Y.L.; translating, Y.R.; review and editing, L.L. All authors have read and agreed to the published version of the manuscript.

Funding: This study was supported by the National Science and Technology Infrastructure-The National Infrastructure of Mineral, Rock and Fossil Resources for Science and Technology (<http://www.nimrf.net.cn>, accessed on 25 December 2021), as well as the Program of the Data Integration and Standardization in the Geological Science and Technology from MOST, China, grant number 2013FY110900-3. Chuchu Song also thanks the College Student Research Innovation Program of China University of Geosciences, Beijing.

Data Availability Statement: Data are contained within the article and supplementary materials.

Acknowledgments: We would like to thank the laboratory of the School of Gemology, China University of Geosciences, Beijing, for their help with this experiment.

Conflicts of Interest: The authors declare no conflict of interest.

References

1. Warner, T.E.; Hutzen Andersen, J. The effects of sulfur intercalation on the optical properties of artificial ‘hackmanite’, $\text{Na}_8[\text{Al}_6\text{Si}_6\text{O}_{24}] \text{Cl}_{1.8}\text{S}_{0.1}$; ‘sulfosodalite’, $\text{Na}_8[\text{Al}_6\text{Si}_6\text{O}_{24}] \text{S}$; and natural tugtupite, $\text{Na}_8[\text{Be}_2\text{Al}_2\text{Si}_8\text{O}_{24}] (\text{Cl}, \text{S})_{2-\delta}$. *Phys. Chem. Miner.* **2012**, *39*, 163–168. [[CrossRef](#)]
2. Norrbo, I.; Gluchowski, P.; Paturi, P.; Sinkkonen, J.; Lastusaari, M. Persistent Luminescence of Tenebrescent $\text{Na}_8\text{Al}_6\text{Si}_6\text{O}_{24}(\text{Cl}, \text{S})_2$: Multifunctional Optical Markers. *Inorg. Chem.* **2015**, *54*, 7717–7724. [[CrossRef](#)] [[PubMed](#)]
3. Chukanov, N.V.; Shchipalkina, N.V.; Shendrik, R.Y.; Vigasina, M.F.; Tauson, V.L.; Lipko, S.V.; Varlamov, D.A.; Shcherbakov, V.D.; Sapozhnikov, A.N.; Kasatkin, A.V.; et al. Isomorphism and Mutual Transformations of S-Bearing Components in Feldspathoids with Microporous Structures. *Minerals* **2022**, *12*, 1456. [[CrossRef](#)]
4. Taylor, M.J.; Marshall, D.J.; Evans, H.W. Infra-red spectra of photochromic sodalites. *J. Phys. Chem. Solids* **1971**, *32*, 2021–2026. [[CrossRef](#)]
5. Hu, X.; Peng, T.; Sun, H.; Xie, R.; Xian, H.; Song, P. Effects of Cs Doping on Structural and UV-photochromic Properties of Sodalite. *J. Chin. Ceram. Soc.* **2016**, *3*, 111–119.
6. Norrbo, I.; Gluchowski, P.; Hyppänen, I.; Laihininen, T.; Laukkanen, P.; Mäkelä, J.; Mamedov, F.; Santos, H.S.; Sinkkonen, J.; Tuomisto, M.; et al. Mechanisms of Tenebrescence and Persistent Luminescence in Synthetic Hackmanite $\text{Na}_8\text{Al}_6\text{Si}_6\text{O}_{24}(\text{Cl}, \text{S})_2$ (Article). *ACS Appl. Mater. Interfaces* **2016**, *8*, 11592–11602. [[CrossRef](#)] [[PubMed](#)]
7. Hassan, I.; Antao, M.S.; Parise, B.J. Sodalite: High-temperature structures obtained from synchrotron radiation and Rietveld refinements. *Am. Mineral.* **2004**, *89*, 359–364. [[CrossRef](#)]
8. Radomskaya, T.A.; Kaneva, E.V.; Shendrik, R.Y.; Suvorova, L.F.; Vladyskin, N.V. Sulfur-Bearing Sodalite, Hackmanite, in Alkaline Pegmatites of the Inagli Massif (Aldan Shield): Crystal Chemistry, Photochromism, and Luminescence. *Geol. Ore Depos.* **2021**, *63*, 696–704. [[CrossRef](#)]
9. Kaiheriman, M.; Maimaitinai, A.; Rehiman, A.; Sidike, A. Photoluminescence properties of green and red luminescence from natural and heat-treated sodalite. *Phys. Chem. Miner.* **2014**, *41*, 227–235. [[CrossRef](#)]
10. Byron, H.; Kreivilä, T.; Colinet, P.; Le Bahers, T.; Lastusaari, M. New shades of photochromism—Yellow sodalites for the detection of blue light. *J. Mater. Chem. C* **2023**, *11*, 3360–3374. [[CrossRef](#)]
11. Hassib, A.; Beckman, O.; Annersten, H. Photochromic properties of natural sodalite. *J. Physics. D Appl. Phys.* **1977**, *10*, 771–777. [[CrossRef](#)]
12. Pizani, P.S.; Terrile, M.C.; Farach, H.A.; Poole, C.P. Color centers in sodalite. *Am. Mineral.* **1985**, *70*, 1186–1192.
13. Warner, T.E. Artificial Hackmanite $\text{Na}_8[\text{Al}_6\text{Si}_6\text{O}_{24}] \text{Cl}_{1.8}\text{S}_{0.1}$ by a Structure-Conversion Method with Annealing Under a Reducing Atmosphere. *Synth. Prop. Mineral. Important Inorg. Mater.* **2011**, 240–253. [[CrossRef](#)]
14. Van Doorn, C.Z.; Schipper, D.J. Luminescence of O^{2-} , Mn^{2+} and Fe^{3+} in sodalite. *Phys. Lett. A* **1971**, *34*, 139–140. [[CrossRef](#)]
15. Blumentritt, F.; Vigier, M.; Fga, E.F. Blue Persistent Luminescence (Phosphorescence) of Sodalite. *J. Gemmol.* **2021**, *37*, 571–574. [[CrossRef](#)]
16. Gaft, M.; Panczer, G.; Nagli, L.; Yeates, H. Laser-induced time-resolved luminescence of tugtupite, sodalite and hackmanite. *Phys. Chem. Miner.* **2009**, *36*, 127–141. [[CrossRef](#)]
17. Zahoransky, T.; Friis, H.; Marks, M. Luminescence and tenebrescence of natural sodalites: A chemical and structural study. *Phys. Chem. Miner.* **2016**, *43*, 459–480. [[CrossRef](#)]
18. Kaneda, T.; Matsumoto, T.; Watanabe, Y. Color change and thermochromism of sodalite, $\text{Na}_8[\text{Al}_6\text{Si}_6\text{O}_{24}] (\text{I}, \text{S})_2$, synthesized by hydrothermal reaction. *Microporous Mesoporous Mater.* **2023**, *355*, 112577. [[CrossRef](#)]
19. Stroud, C.E.; Stencil, J.M.; Todd, L.T. Infrared spectra of cathodochromic sodalite. *J. Phys. Chem.* **1979**, *83*, 2378–2382. [[CrossRef](#)]
20. Zhou, X.T.; Liu, Q.F.; Liu, Y. Ionothermal Synthesis of Sodalite from Metakaolin. *Emerg. Mater. Mech. Appl.* **2012**, *487*, 789–792.
21. Borhade, A.V.; Dholi, A.G. Synthesis and crystal structure of chlorate-enclathrated in aluminogermanate sodalite $\text{Na}_8[\text{AlGeO}_4]_6 (\text{ClO}_3)_2$ (Article). *Mater. Sci. Pol.* **2013**, *31*, 246–252. [[CrossRef](#)]
22. Liu, X.; Thomas, J.K. New absorption band in the mid-infrared spectra of Cd^{2+} -exchanged zeolites. *Chem. Phys. Lett.* **1988**, *144*, 286–291. [[CrossRef](#)]
23. Henderson, C.M.B.; Taylor, D. Infrared spectra of anhydrous members of the sodalite family. *Spectrochim. Acta Part A Mol. Spectrosc.* **1977**, *33*, 283–290. [[CrossRef](#)]
24. Mofrad, A.M.; Schellenberg, P.S.; Peixoto, C.; Hunt, H.K.; Hammond, K.D. Calculated infrared and Raman signatures of Ag^+ , Cd^{2+} , Pb^{2+} , Hg^{2+} , Ca^{2+} , Mg^{2+} , and K^+ sodalites. *Microporous Mesoporous Mater.* **2020**, *296*, 109983. [[CrossRef](#)]
25. Bolotina, N.B.; Sapozhnikov, A.N.; Chukanov, N.V.; Vigasina, M.F. Structure Modulations and Symmetry of Lazurite-Related Sodalite-Group Minerals. *Crystals* **2023**, *13*, 768. [[CrossRef](#)]
26. Borhade, A.V.; Dholi, A.G.; Kshirsagar, T.A. Synthesis and Characterization of a New Aluminogermanate Thiocyanate Aluminogermanate Sodalite $\text{Na}_8[\text{AlGeO}_4]_6(\text{SCN})_2$. *Russ. J. Phys. Chem. A* **2020**, *94*, 370–375. [[CrossRef](#)]
27. Henderson, C.M.B.; Taylor, D. Infrared spectra of aluminogermanate- and aluminate-sodalites and a re-examination of the relationship between T-O bond length, T-O-T angle and the position of the main i.r. absorption band for compounds with framework structures. *Spectrochim. Acta Part A* **1979**, *35*, 929–935. [[CrossRef](#)]
28. Chukanov, N.V.; Aksenov, S.M.; Pekov, I.V. Infrared spectroscopy as a tool for the analysis of framework topology and extra-framework components in microporous cancrinite- and sodalite-related aluminosilicates. *Spectrochim. Acta Part A Mol. Biomol. Spectrosc.* **2022**, *287*, 121993. [[CrossRef](#)]

29. Armstrong, J.A.; Weller, M.T. Structural observation of photochromism. *Chem. Commun.* **2006**, *10*, 1094–1096. [[CrossRef](#)]
30. Ariai, J.; Smith, S.R.P. The Raman spectra and analysis of phonon modes in sodalite. *J. Phys. C Solid State Phys.* **1981**, *14*, 1193. [[CrossRef](#)]
31. Badrinarayan, M.K.; Stencel, J.M.; Todd, L.T., Jr. Raman scattering study of the coloration mechanism of cathodochromic sodalite. *J. Phys. Chem.* **1980**, *84*, 456–459. [[CrossRef](#)]
32. Naqvi, A.S.; Naveedullah, K.; Hamdan, J.M. Raman scattering studies of sodalite for crystal structure and coloration mechanism. *Il Nuovo Cimento D* **1991**, *13*, 21–29. [[CrossRef](#)]
33. Sidike, A.; Sawuti, A.; Wang, X.M.; Zhu, H.J.; Kobayashi, S.; Kusachi, I.; Yamashita, N. Fine structure in photoluminescence spectra of S^{2-} center in sodalite. *Phys. Chem. Miner.* **2007**, *34*, 477–484. [[CrossRef](#)]
34. Norrbo, I.; Hyppänen, I.; Lastusaari, M. Up-conversion luminescence—A new property in tenebrescent and persistent luminescent hackmanites (Article). *J. Lumin.* **2017**, *191*, 28–34. [[CrossRef](#)]
35. Cano, N.; Blak, A.R.; Watanabe, S. Correlation between electron paramagnetic resonance and thermoluminescence in natural sodalite. *Phys. Chem. Miner.* **2010**, *37*, 57–64. [[CrossRef](#)]
36. Annersten, H.; Hassib, A. Blue sodalite. *Can. Miner.* **1979**, *17*, 39–46.

Disclaimer/Publisher’s Note: The statements, opinions and data contained in all publications are solely those of the individual author(s) and contributor(s) and not of MDPI and/or the editor(s). MDPI and/or the editor(s) disclaim responsibility for any injury to people or property resulting from any ideas, methods, instructions or products referred to in the content.